nature nanotechnology

LETTERS

PUBLISHED ONLINE: 21 DECEMBER 2008 | DOI: 10.1038/NNANO.2008.373

One-step DNA-programmed growth of luminescent and biofunctionalized nanocrystals

Nan Ma[1], Edward H. Sargent[2] and Shana O. Kelley[1,3]*

Colloidal semiconductor nanocrystals are widely used as lumiphores in biological imaging because their luminescence is both strong and stable, and because they can be biofunctionalized. During synthesis, nanocrystals are typically passivated with hydrophobic organic ligands[1], so it is then necessary either to replace these ligands or encapsulate the nanocrystals with hydrophilic moieties to make the lumiphores soluble in water. Finally, biological labels must be added to allow the detection of nucleic acids, proteins and specific cell types[2–8]. This multistep process is time- and labour-intensive and thus out of reach of many researchers who want to use luminescent nanocrystals as customized lumiphores. Here, we show that a single designer ligand—a chimeric DNA molecule—can controllably program both the growth and the biofunctionalization of the nanocrystals. One part of the DNA sequence controls the nanocrystal passivation and serves as a ligand, while another part controls the biorecognition. The synthetic protocol reported here is straightforward and produces a homogeneous dispersion of nanocrystal lumiphores functionalized with a single biomolecular receptor. The nanocrystals exhibit strong optical emission in the visible region, minimal toxicity and have hydrodynamic diameters of ~6 nm, which makes them suitable for bioimaging[4]. We show that the nanocrystals can specifically bind DNA, proteins or cells that have unique surface recognition markers.

DNA is well suited to the task of producing customized nanocrystal lumiphores because it is known to serve as a receptor for molecular recognition[9] and as an inert nanocrystal passivator[10–15]. Both nucleic acids sequence and structure have been used to control the properties of lead- and cadmium-containing nanocrystals[13,14], and the materials made in this way have been shown to have low cellular toxicity and good properties for cellular imaging[13]. However, little has been done to functionalize these materials to enable versatile molecular recognition. An aptamer-based strategy using DNA for both nanoparticle liganding during growth and protein detection has recently been reported[15]; the toxicities and hydrodynamic radii of these materials were not investigated, and although the proposed application of the strategy was restricted to a single protein, adsorption of non-target proteins was noted. In summary, although promising advances have already been made, a general approach to high-fidelity biomolecular functionalization of nanocrystals capable of specifically binding to a diverse range of targets has never previously been explored.

We designed a one-pot synthesis that would allow nucleic acids-functionalized nanocrystals to be prepared that would bind a variety of biomolecular targets. The approach relies on the design of chimeric oligonucleotides that contain two different domains—one that will be liganded to the nanocrystal, and one that will be capable of molecular recognition (Fig. 1). Our demonstration herein of strong and specific binding to a wide diversity of

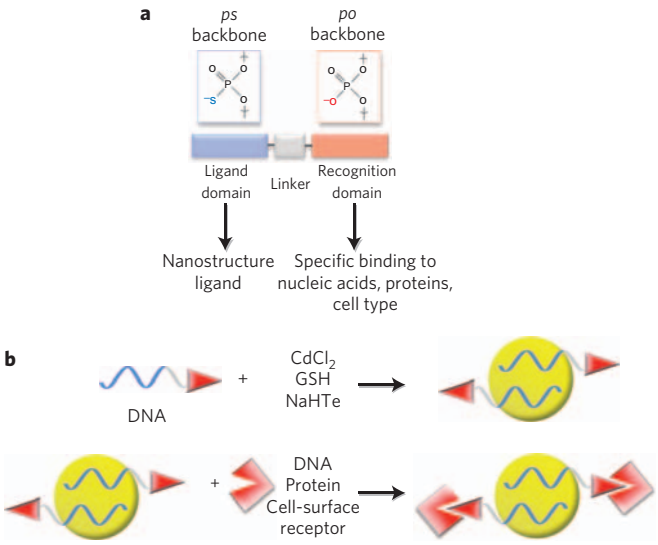

Figure 1 | Strategy for one-pot synthesis of DNA-functionalized CdTe nanocrystals. a, Design of chimeric oligonucleotides with a ligand domain (phosphorothioate, blue) and a recognition domain (phosphate, red). **b**, One-pot synthesis of DNA-functionalized CdTe nanocrystals using DNA, $CdCl_2$, NaHTe and glutathione (GSH) as precursors. The phosphorothioate portion of the sequence (blue) serves as a nanocrystal ligand, while the phosphate portion (red) of the DNA sequence remains free to bind to biomolecular partners.

targets—DNA, proteins and cells—stems directly from this chimeric strategy, in which one portion is optimized for liganding, and the other is optimized for interaction with biomolecular targets. To produce one oligonucleotide structure that would be able to contain both types of moieties, we proposed building oligonucleotides containing two different types of backbones with different affinities for metals. Phosphorothioates (*ps*), sulphur-containing variants of the usual phosophodiester backbone, were used to provide a ligand structure that would preferentially bind an inorganic surface over phosphates (*po*)[16]. Cd^{2+} ions are known to exhibit a 3,000-fold preference for sulphur over oxygen binding when presented with nucleotides; thus we believed that this preferential binding would direct the two domains to interact with the nanocrystal surface to very different extents. By including both *po* and *ps* backbones in one oligonucleotide, DNA would serve as a ligand for, and an appendage to, the nanocrystal synthesized in its presence.

To produce DNA-functionalized nanocrystals that would be of maximal utility for imaging applications, we developed a synthetic

[1]Department of Pharmaceutical Sciences, Leslie Dan Faculty of Pharmacy, University of Toronto, Toronto, Ontario M5S 3M2, Canada, [2]Department of Electrical and Computer Engineering, Faculty of Engineering, University of Toronto, Toronto, Ontario M5S 3M2, Canada, [3]Department of Biochemistry, Faculty of Medicine, University of Toronto, Toronto, Ontario M5S 3M2, Canada; *e-mail: shana.kelley@utoronto.ca

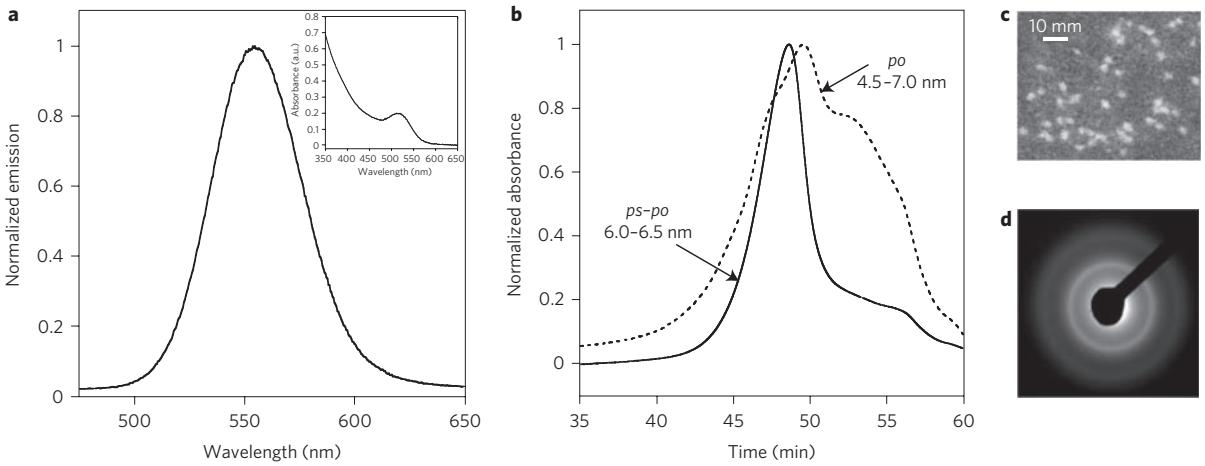

Figure 2 | Characterization of DNA-functionalized CdTe nanocrystals. a, Emission spectrum and absorption spectrum (inset) of DNA-functionalized CdTe quantum dots (QDs). **b**, Sizing of *ps–po* DNA and all *po* DNA-passivated CdTe QDs using gel filtration chromatography. (See Supplementary Information for sizing standards.) **c**, Dark-field transmission electron microscopy (TEM) image of CdTe made with *ps–po* DNA. **d**, Selected area diffraction (SAD) image of CdTe made with *ps–po* DNA.

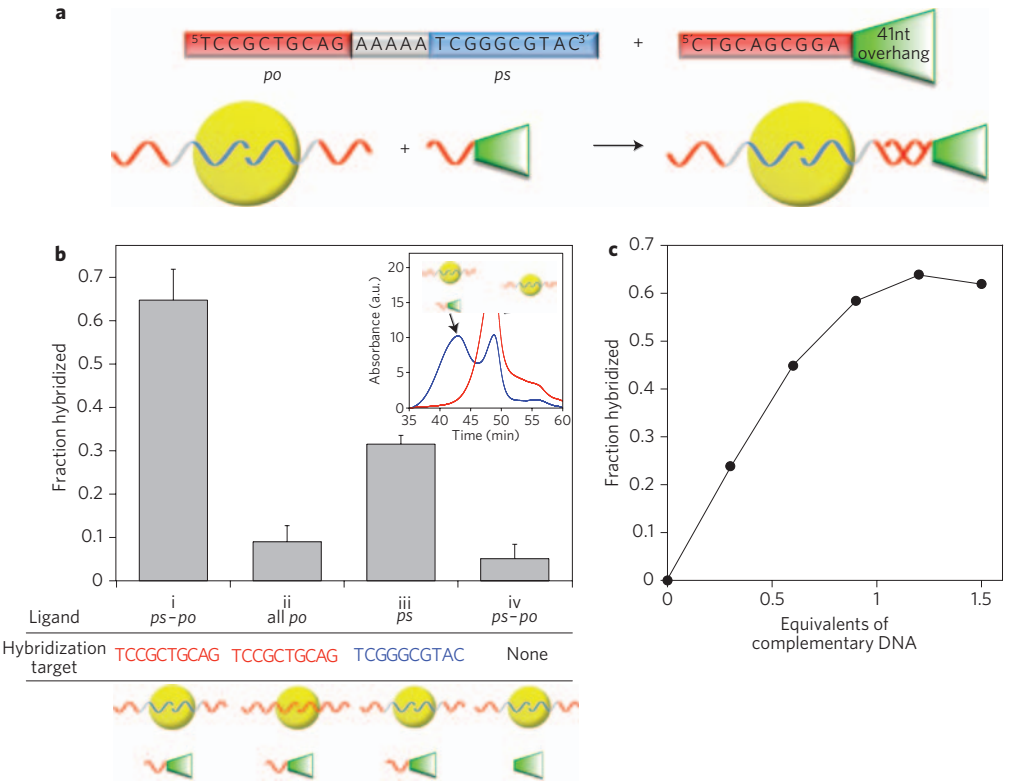

Figure 3 | Hybridization of DNA-functionalized CdTe nanocrystals with complementary DNA. a, Sequences of *ps–po* DNA and target DNA and schematic diagram of hybridization reaction. **b**, Fraction hybridized for different DNA–CdTe constructs calculated using gel filtration chromatography (inset). From left to right: (i) *ps–po*–CdTe with target DNA complementary to *po* portion; (ii) all *po*–CdTe with target DNA complementary to *po* portion; (iii) *ps–po*–CdTe with target DNA complementary to *ps* portion; (iv) *ps–po*–CdTe with non-complementary target DNA. Error bars are standard deviations from multiple trials. **c**, Determination of number of available binding sites on DNA–CdTe. The introduction of differing stoichiometries of a complementary sequence indicates that one immobilized oligonucleotide is available for binding, as saturation of binding is observed when a 1:1 ratio is reached.

protocol that would yield strongly emissive materials. We took as our starting point a method previously developed for the synthesis of CdTe that uses glutathione (GSH) as a ligand and sulphur source[17]; the synthesis is compatible with the use of water as a solvent, and is conducted under ambient atmosphere at 100 °C. Given that DNA is stable under these conditions, this appeared to be an ideal strategy for incorporation of DNA as a co-ligand. In the presence of a chimeric *ps–po* DNA oligonucleotide, the CdTe nanocrystals generated using this approach have desirable emission properties, demonstrating 17% quantum yield and a full-width at half-maximum of 50 nm (Fig. 2a). The emission spectrum of DNA–CdTe relative to nanocrystals made with GSH alone is

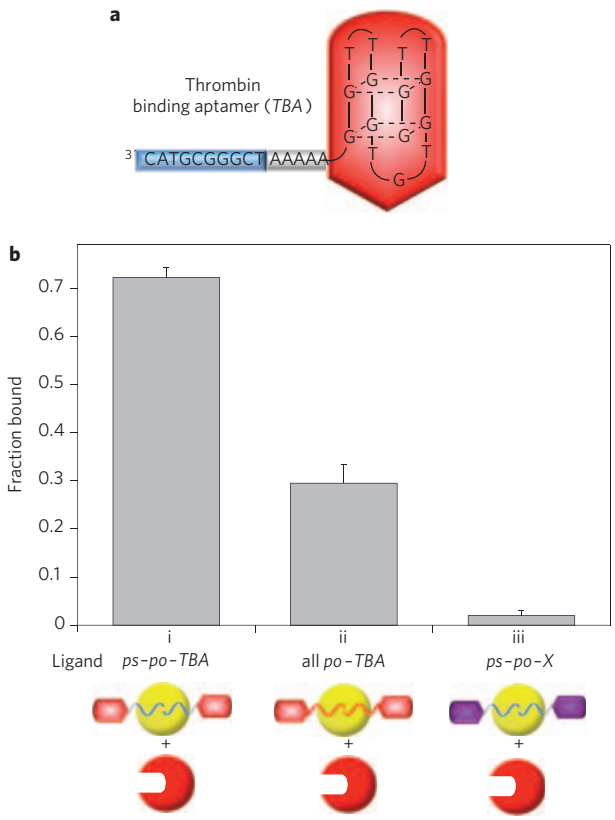

Figure 4 | Binding of thrombin to CdTe nanocrystals functionalized with the thrombin-binding aptamer monitored using gel filtration chromatography. a, Sequence of chimeric DNA with thrombin binding aptamer (red) as the recognition domain and phosphorothioate DNA (blue) as the ligand domain. **b**, Fraction bound for different DNA–CdTe constructs. From left to right: (i) *ps–po–TBA*–CdTe with thrombin; (ii) all *po–TBA*–CdTe with thrombin; (iii) *ps–po–X*–CdTe with thrombin (*X* is a non-cognate sequence for thrombin). Error bars are standard deviations from multiple trials.

blueshifted, indicating that the DNA ligand may interact electronically with the crystal surface and alter its electronic properties. Transmission electron microscopy (TEM) images confirm that the materials are nanoscale, and selected area diffraction (SAD) confirms that they are crystalline (Fig. 2).

The hydrodynamic size of the DNA-functionalized nanocrystals was assessed using gel filtration chromatography (Fig. 2b). Sizing standards were used to calibrate the experiment and allow for the calculation of diameters (see Supplementary Information). CdTe made with the *ps–po* oligonucleotide exhibited small hydrodynamic diameters with a narrow size distribution ranging from 6.0 to 6.5 nm as measured by gel filtration chromotagraphy. Those made with GSH alone had diameters of 4.3 to 5.3 nm (see Supplementary Information, Fig. S1 and ref. 17), illustrating that functionalization was achieved without an excessive increase in the overall size of the nanocrystals. Obtaining nanocrystals in this size range is ideal, as circulation in living systems has been shown to be impeded for structures with larger hydrodynamic diameters[4]. To examine the role of the *ps* backbone as a ligand, we also analysed products of syntheses performed with all *po* oligonucleotides. Interestingly, CdTe synthesized with all *po* DNA exhibit a much broader size distribution ranging from 4.5 to 7.0 nm (Fig. 2b). This observation suggests that the *ps* domain directs the formation of products that are uniformly sized, but, in the absence of this functionality, products with a variety of ligand conformations and orientations are obtained.

The stability of DNA-functionalized CdTe nanocrystals was also assessed to determine whether these materials would withstand different incubation conditions. High pH and high ionic strength were not found to perturb the emission of the nanocrystals, but it was determined that low pH strongly diminished the luminescence (see Supplementary Information). Nonetheless, the nanomaterials produced are stable under the conditions that would be of most utility for biological studies.

To evaluate the binding of the DNA-passivated CdTe nanocrystals to biomolecular targets, we first tested the hybridization with complementary DNA using gel filtration chromatography (Fig. 3). The DNA target used contains a 10-nucleotide binding sequence and a 41-nucleotide overhang, and the hybridization was carried out for 60 minutes at room temperature. For the CdTe synthesized with *ps–po* DNA and hybridized with the DNA target complementary to the *po* domain, a high level of hybridization was achieved. However, when an all-*po* DNA oligomer with the same sequence was used for CdTe synthesis, hybridization was strongly diminished. This dramatic difference suggests that it is necessary to incorporate the *ps* domain into the ligand DNA to allow the *po* domain to be free for binding. In order to confirm further that the *ps* domain was more strongly liganded to the nanocrystal than the *po* domain, the hybridization of a DNA target complementary to the *ps* portion was monitored. A significant decrease in hybridization efficiency was observed, indicating that most of the *ps* domains present are interacting with the surface of the nanocrystals as ligands, with the *po* portion much more accessible for hybridization. DNA targets lacking any complementarity to the *ps–po* oligonucleotide displayed no binding, confirming that the complexation observed is specific. The number of DNA oligonucleotides available for binding to complementary targets was also assessed by titrating DNA–CdTe with differing stoichiometries of complement, and it was found, interestingly, that only one DNA sequence is available for binding per nanocrystal (Fig. 3c).

The binding of DNA-functionalized CdTe to protein targets was also explored. We used the thrombin binding aptamer (*TBA*) to explore the binding of a model protein target. This aptamer was discovered using *in vitro* selection and folds into a G-quartet structure which binds to either the fibrinogen recognition exosite or the heparin binding site of thrombin[18,19]. Thus, we designed a chimeric DNA oligonucleotide with *TBA* as the *po*-based recognition domain and a *ps* portion as the ligand domain (*ps–po–TBA*). This chimeric DNA was used as a co-ligand during synthesis and the binding of CdTe with thrombin was then monitored by gel filtration chromatography. As shown in Fig. 4, the nanocrystals synthesized with *ps–po–TBA* exhibit the highest binding level towards thrombin and there is no non-specific binding of thrombin to the CdTe synthesized with a scrambled DNA aptamer (*ps–po–X*). When all *po–TBA* is used to replace *ps–po–TBA* for CdTe synthesis, a much lower binding level is observed, but it is higher than the binding to DNA shown in Fig. 3. However, this small amount of binding appears to be non-specific, as when binding of all *po* CdTe to bovine serum albumin (BSA) was evaluated, significant complexation was observed (see Supplementary Information) that was much higher than obtained when a *ps–po* sequence was used for synthesis. It is likely that the high levels of non-specific adsorption result from displacement of the poorly bound DNA phosphate ligands by protein residues. These results further illustrate that integrating a *ps* domain, with the phosphorothioate providing strongly bound ligands that are less susceptible to displacement, into a DNA ligand is important in the generation of bioactive and specific CdTe.

The results of research aimed at constructing DNA-passivated CdTe with high fidelity and specificity toward nucleic acids and protein targets suggests that, potentially, these materials could be applied to much more complicated systems such as live cells for imaging and diagnostic applications. To test the suitability of our

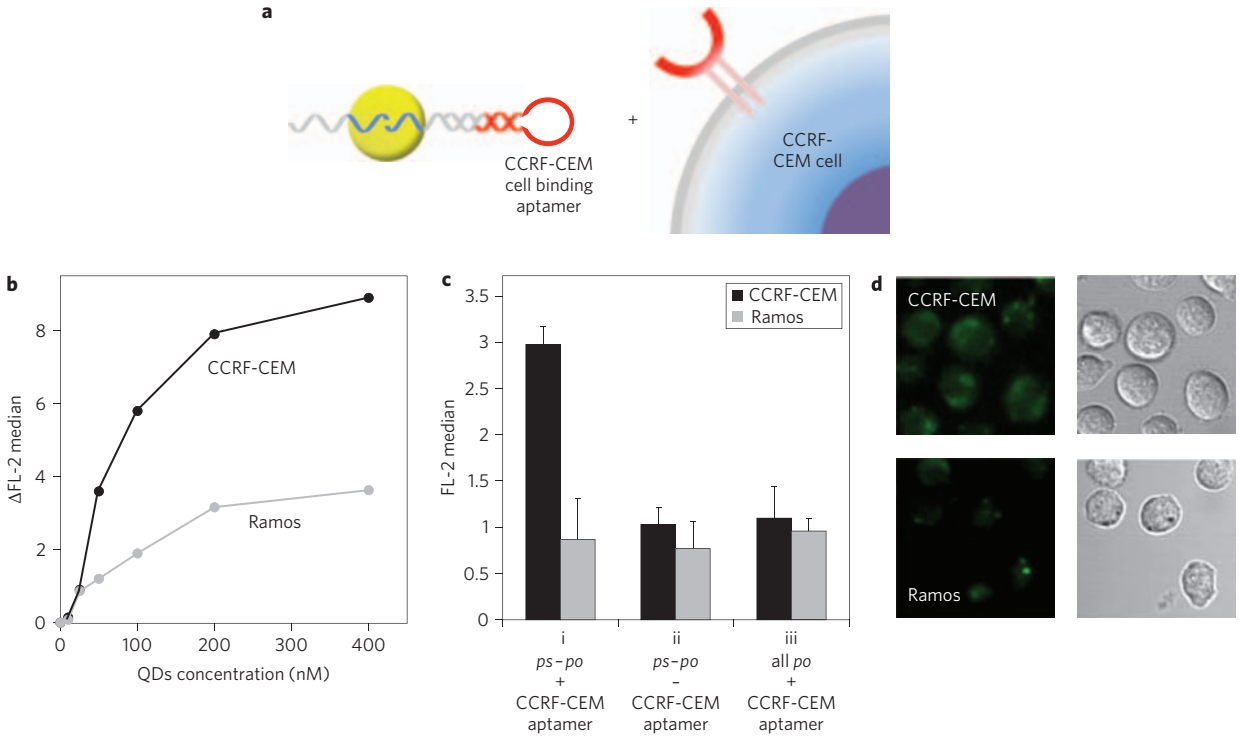

Figure 5 | Specific binding of CdTe nanocrystals functionalized with a cell-binding aptamer to cognate cells. a, Schematic diagram of cell binding aptamer-functionalized CdTe QD and its binding with the cell surface receptor of a CCRF-CEM cell. **b**, Binding curves for cell binding aptamer-functionalized CdTe QDs bound to CCRF-CEM and Ramos cells measured by monitoring changes in fluorescence median using flow cytometry. **c**, Comparison of cell binding for CdTe QDs (i) functionalized with the *ps–po* sequence and then hybridized to the cell binding aptamer, (ii) functionalized with the *ps–po* sequence but lacking the aptamer and (iii) made with the all *po* sequence and incubated with the cell-binding aptamer. Background binding of GSH–CdTe QDs with CCRF-CEM cells and Ramos cells have been subtracted. **d**, Confocal imaging of CCRF-CEM cells and Ramos cells bound with cell binding aptamer-functionalized CdTe QDs. Upper left, fluorescence image of CCRF-CEM cells; upper right, differential interference constrast (DIC) image of CCRF-CEM cells; lower left, fluorescence image of Ramos cells; lower right, DIC image of Ramos cells.

materials for this application, we examined DNA-programmed CdTe nanocrystals functionalized with a cancer-cell binding aptamer. These recently discovered aptamers represent an attractive alternative to routinely used antibodies because of their small sizes, chemical robustness and ease of synthesis[20–23]. We selected an aptamer previously shown to exhibit selective affinity to CCRF-CEM cells (T cell line, human acute lymphoblastic leukaemia) versus Ramos cells (B cell line, human Burkitt's lymphoma). To functionalize our CdTe with the cell binding aptamer, a *ps–po* DNA oligomer was used to synthesize CdTe, and then the cell-binding aptamer carrying a sequence complementary to the *po* portion was introduced to CdTe through hybridization. Binding with live CCRF-CEM cells and Ramos cells was then monitored by flow cytometry and fluorescence microscopy. As shown in Fig. 5, the aptamer-functionalized CdTe exhibits detectable discrimination between the two cell types. Importantly, we confirmed that the aptamer is responsible for the cell-type discrimination by also monitoring the construct lacking the hybridized aptamer or made with an all *po* sequence (Fig. 5c); these materials did not exhibit appreciable differential binding to the two cell types. Fluorescence imaging of aptamer-functionalized CdTe also shows qualitatively that there is differential binding to CCRF-CEM and Ramos cells. These results indicate that using a one-pot aqueous synthesis with simple and accessible materials, imaging agents can be prepared that are cell-type specific.

The applicability of these DNA-functionalized CdTe nanocrystals to biological studies requires that their presence have a minimal effect on cellular function and viability. To assess directly the toxicity of our materials, we monitored the viability of the CCRF-CEM cells that are specifically bound by aptamer-modified CdTe. No appreciable cell death was observed (see Supplementary Information), indicating that the materials are stable and not prone to releasing components when introduced into biological media.

In summary, we have developed a strategy that allows the simultaneous synthesis and functionalization of CdTe nanocrystals through a convenient one-pot process by using chimeric DNA molecules as ligands. These DNA-passivated nanocrystals exhibit high specific binding to nucleic acids, protein and cell targets. Moreover, they are non-toxic and possess small hydrodynamic radii; these are essential qualities for biological imaging applications.

Methods

Materials. Cadmium sulphide, tellurium powder, sodium borohydride, GSH and human α-thrombin were purchased from Sigma-Aldrich and used as received. DNA was purchased from Integrated DNA Technologies. Protein standards for nanocrystals sizing including blue dextran, thyroglobulin, BSA and lysozyme were from Sigma-Aldrich. CCRF-CEM (CCL-119, T-cell line, human ALL) and Ramos (CRL-1596, B cell line, human Burkitt's lymphoma) were from American Type Culture Collection (ATCC). Both cell lines were cultured in RPMI 1640 medium supplemented with 10% heat-inactivated fetal bovine serum (GIBCO) and 100 units ml^{-1} penicillin–streptomycin (Cellgro) in a humidified incubator at 37 °C containing 5% CO_2. Cell binding buffer was prepared by dissolving 0.9 g glucose (Sigma), 0.2033 g magnesium chloride hexahydrate (Sigma), 20 mg yeast tRNA (Sigma) and 200 mg BSA in 200 ml 1× Dulbecco's PBS (with $MgCl_2$ and $CaCl_2$) supplemented with 10% FBS (heat inactivated).

DNA sequences. *ps–po*: 5′TCCGCTGCAGAAAAAT*C*G*G*C*G*T*A*C3′ (* indicates phosphorothioate linkage)

All *po*: 5′TCCGCTGCAGAAAAATCGGGCGTAC3′DNA target complementary to *po*: 5′CTGCAGCGGAATCTAACTGCTGCGCCGCCGGGAAAATACTGTACGGTTAGA3′

DNA target complementary to *ps* portion: 5′ATCTAACTGCTGCGCCGCCGGGAAAATACTGTACGGTTAGAGTACGCCCGA3′

Non-complementary DNA target: 5′ATCTAACTGCTGCGCCGCCGGGAAAA TACTGTACGGTTAGA3′

ps–po–TBA: 5′GGTTGGTGTGGTTGGAAAAAT*C*G*G*G*C*G*T*A*C3′

All *po–TBA*: 5′GGTTGGTGTGGTTGGAAAAATCGGGCGTAC3′

ps–po–X: 5′TCCGCTGCAGAAAAAT*C*G*G*G*C*G*T*A*C3′

Cell binding aptamer carrying a sequence complementary to *po* portion of *ps–po*: 5′CTGCAGCGGAATCTAACTGCTGCGCCGCCGGGAAAATACTGTACGGT TAGA3′

Functionalized CdTe synthesis and characterization. Sodium hydrogen telluride (NaHTe) was freshly made before each synthesis by dissolving 0.025 g sodium borohydride ($NaBH_4$) in 1 ml deionized water and then 0.040 g tellurium powder was added into the $NaBH_4$ solution. This reaction was conducted at room temperature overnight in an eppendorf tube with a needle ($21G1^1/_2$, BD) inserted through the lid to help release the gas generated during the reaction. $CdCl_2$-GSH stock solution was made to include 1.25 mM $CdCl_2$ and 1.05 mM GSH in H_2O and pH was adjusted to 9.0 with sodium hydroxide before use. For a typical CdTe synthesis, 400 μl $CdCl_2$-GSH stock solution was mixed with 0.8 μl of freshly prepared NaHTe solution in a 0.7 ml eppendorf tube and then DNA solution containing 120 nmol nucleotides was added. The reaction was conducted on a heat block (Fisher Scientific) at 100 °C for 1 h and then gradually cooled to room temperature. The absorption and emission spectra of CdTe were taken on Agilent 8453 absorption spectrophotometer and HR2000 fibre optic emission spectrometer, respectively. Quantum yields were measured using 9,10-diphenylanthracene (Sigma) in hexane as a relative standard with an excitation wavelength of 375 nm and an integrated emission between 380 and 900 nm. For nanocrystals sizing, a protein standards solution was prepared to include 15 μl blue dextran (25 mg ml^{-1}), 35 μl thyroglobulin (25 mg ml^{-1}), 25 μl BSA (25 mg ml^{-1}) and 10 μl lysozyme (25 mg ml^{-1}). Gel filtration chromatography was run using a Superose 10/300GL column (Amersham). The flow rate was fixed at 0.35 ml min^{-1} and each sample ran for an overall time of 80 min. The wavelength used to monitor nanocrystals was set at 370 nm and recorded by HP 1100 HPLC system. 1× Dulbecco's PBS (pH 7.4) was used as running buffer.

Transmission electron microscopy and selected area diffraction. TEM images were taken using Hitachi HD-2000 scanning transmission electron microscope (STEM) in annular dark-field mode at 200 kV. CdTe QDs were filtered through Microcon YM-50 centrifugal filters and resuspended in water to remove free ligands and then 5 μl of sample was dispensed onto a 3 mm copper grid covered with a continuous carbon film. The samples were air-dried at room temperature.

Binding of nanocrystals with DNA and protein targets. The quantitation of CdTe–DNA was performed using an approximate extinction coefficient of 200,000 cm^{-1} M^{-1} at 520 nm according to ref. 24. Free DNA targets were quantitated using an extinction coefficient of 489,700 cm^{-1} M^{-1} at 260 nm.

For DNA binding, 1.5-fold excess DNA targets were added into CdTe-containing solutions and left at room temperature for 1 h before gel filtration chromatography measurements. For protein binding, human α-thrombin and BSA were dissolved in 1× Dulbecco's PBS and 1.5-fold excess protein targets were added into CdTe solutions containing 0.5× Dulbecco's PBS, which was then incubated at 37 °C for 1 h. The binding was monitored by gel filtration chromatography and the binding fraction was calculated by integrating the area of each peak. For binding of nanocrystals with cells, to functionalize CdTe with a cell-binding aptamer, CdTe synthesized with *ps–po* DNA (400 μl) were first purified using a Microcon YM-50 centrifugal filter (8,000*g*, 10 min) to remove excess DNA and ions. Then the CdTe particles were resuspended in 400 μl of 10 mM $MgCl_2$ solution containing 4 μM cell binding aptamer carrying the sequence complementary to the *po* portion. The hybridization reaction was carried out at room temperature for 1 h. Functionalized CdTe were buffer exchanged using a Microcon YM-50 centrifugal filter by resuspending the CdTe in 400 μl cell binding buffer. For each binding, 1×10^6 cells were suspended in 400 μl CdTe solution and incubated at 4 °C for 1 h. Unbound CdTe was removed by spinning down the cell suspension and the cells were washed twice with ice-cold cell binding buffer. The cell binding was monitored using a BD FACSCalibur flow cytometer with 488 nm laser excitation. CdTe synthesized with GSH alone was used to evaluate background binding. The CdTe synthesized with *ps–po* DNA without further functionalization were used as non-cognate aptamer binding control.

Confocal microscopy. 1×10^5 CCRF-CEM or Ramos cells were suspended in 300 μl cell binding buffer containing 200 nM of cell-binding aptamer-functionalized CdTe and incubated at 4 °C for 1 h. The cells were then recollected by centrifugation and washed twice with ice-cold cell binding buffer. The photoluminescence images were obtained with a Zeiss LSM 510 confocal microscope using a ×63 water immersion objective with 488 nm argon laser excitation and the emission was collected with a 505 nm long-pass filter. Microscope settings were adjusted to eliminate autofluorescence and kept constant during acquisition.

Received 13 October 2008; accepted 18 November 2008; published online 21 December 2008

References

1. Murray, C. B., Norris, D. J. & Bawendi, M. G. Synthesis and characterization of nearly monodisperse CdE (E = S, Se, Te) semiconductor nanocrystallites. *J. Am. Chem. Soc.* **115,** 8706–8715 (1993).
2. Chan, W. C. W. & Nie, S. Quantum dot bioconjugates for ultrasensitive nonisotopic detection. *Science* **281,** 2016–2018 (1998).
3. Gao, X., Cui, Y., Levenson, R. M., Chung, L. W. K. & Nie, S. *In vivo* cancer targeting and imaging with semiconductor quantum dots. *Nature Biotechnol.* **22,** 969–976 (2004).
4. Choi, H. S. *et al.* Renal clearance of quantum dots. *Nature Biotechnol.* **25,** 1165–1170 (2007).
5. Pathak, S., Choi, S.-K., Arnheim, N. & Thompson, M. E. Hydroxylated quantum dots as luminescent probes for *in situ* hybridization. *J. Am. Chem. Soc.* **123,** 4103–4104 (2001).
6. Michalet, X. *et al.* Quantum dots for live cells, *in vivo* imaging and diagnostics. *Science* **307,** 538–544 (2005).
7. Medintz, I. L., Uyeda, H. T., Goldman, E. R. & Mattoussi, H. Quantum dot bioconjugates for imaging, labeling and sensing. *Nature Mater.* **4,** 435–446 (2005).
8. Dubertret, B. *et al. In vivo* imaging of quantum dots encapsulated in phospholipid micelles. *Science* **298,** 1759–1762 (2002).
9. Yan, A. C, Bell, K. M., Breeden, M. M. & Ellington, A. D. Aptamers: prospects in therapeutics and biomedicine. *Front. Biosci.* **10,** 1802–1827 (2005).
10. Berti, L. & Burley, G. A. Nucleic acid and nucleotide-mediated synthesis of inorganic nanoparticles. *Nature Nanotech.* **3,** 81–87 (2008).
11. Ma, N., Sargent, E. H. & Kelley, S. O. Biotemplated nanostructures: directed assembly of electronic and optical materials using nanoscale complementarity. *J. Mater. Chem.* **18,** 954–964 (2008).
12. Hinds, S. *et al.* Nucleotide-directed growth of semiconductor nanocrystals. *J. Am. Chem. Soc.* **128,** 64–65 (2006).
13. Ma, N., Yang, J., Stewart, K. M. & Kelley, S. O. DNA-passivated CdS nanocrystals: luminescence, bioimaging and toxicity profiles. *Langmuir* **23,** 12783–12787 (2007).
14. Ma, N., Dooley, C. J. & Kelley, S. O. RNA-templated semiconductor nanocrystals. *J. Am. Chem. Soc.* **128,** 12598–12599 (2006).
15. Choi, J. H., Chen, H. K. & Strano, M. S. Aptamer-capped nanocrystal quantum dots: a new method for label-free protein detection. *J. Am. Chem. Soc.* **128,** 15584–15585 (2006).
16. Pecoraro, V. L., Hermes, J. D. & Cleland, W. W. Stability constants of Mg^{2+} and Cd^{2+} complexes of adenine nucleotides and thionucleotides and rate constants for formation and dissociation of MgATP and MgADP. *Biochemistry* **23,** 5262–5271 (1984).
17. Qian, H., Dong, C., Weng, J. & Ren, J. Facile one-pot synthesis of luminescent, water-soluble and biocompatible glutathione-coated CdTe nanocrystals. *Small* **2,** 747–751 (2006).
18. Bock, L. C., Griffin, L. C., Latham, J. A., Vermaas, E. H. & Toole, J. J. Selection of single-stranded DNA molecules that bind and inhibit human thrombin. *Nature* **355,** 564–566 (1992).
19. Padmanabhan, K., Padmanabhan, K. P., Ferrara, J. D., Sadler, J. E. & Tulinsky, A. The structure of α-thrombin inhibited by a 15-mer single-stranded DNA aptamer. *J. Biol. Chem.* **268,** 17651–17654 (1993).
20. Lupold, S. E., Hicke, B. J., Lin, Y. & Coffey, D. S. Identification and characterization of nuclease-stabilized RNA molecules that bind human prostate cancer cells via the prostate-specific membrane antigen. *Cancer Res.* **62,** 4029–4033 (2002).
21. Cerchia, L. *et al.* Neutralizing aptamers from Whole-Cell SELEX inhibit the RET receptor tyrosine kinase. *PLoS Biol.* **3,** e123 (2005).
22. Shangguan, D. *et al.* Aptamers evolved from live cells as effective molecular probes for cancer study. *Proc. Natl Acad. Sci. USA* **103,** 11838–11843 (2006).
23. Shangguan, D., Tang, Z., Mallikaratchy, P., Xiao, Z. & Tan, W. Optimization and modifications of aptamers selected from live cancer cell lines. *ChemBioChem* **8,** 603–606 (2007).
24. Yu, W. W., Qu, L., Guo, W. and Peng, X. Experimental determination of the extinction coefficient of CdTe, CdSe and CdS nanocrystals. *Chem. Mater.* **15,** 2854–2860 (2003).

Acknowledgements

The authors wish to acknowledge the NIH for support of this work (R21CA122878-02).

Author contributions

N.M. executed all of the experiments reported. All authors participated in the design of the experiments, discussed the results and participated in writing the manuscript.

Additional information

Supplementary Information accompanies this paper at www.nature.com/naturenanotechnology. Reprints and permission information is available online at http://npg.nature.com/reprintsandpermissions/. Correspondence and requests for materials should be addressed to S.O.K.